Symmetry-breaking density profiles in confined liquids

Michael Merkel

Sektion Physik der Universität München, Theresienstraße 37, D-80333 München, Germany

Hartmut Löwen*

Institut für Theoretische Physik II, Universität Düsseldorf, Universitätsstraße 1, D-40225 Düsseldorf, Germany

Density profiles of a liquid confined between two parallel plates are studied near a liquid-gas transition. The system is additionally exposed to an external field depending on the coordinate perpendicular to the plates that possesses a discrete left-right symmetry with respect to the midplane between the plates. It is found that the equilibrium density profiles can be symmetry breaking, i.e., they do not possess the discrete left-right symmetry of the external field. Explicit results are obtained within a simple double-slit model consisting of two layers of two-dimensional Lennard-Jones systems using both computer simulation and density-functional theory. Such symmetry-breaking profiles should be observable in confined colloidal suspensions. [S1063-651X(96)10112-4]

I. INTRODUCTION

If a classical fluid is exposed to an external field with a given symmetry, it is an interesting question whether or not the resulting equilibrium one-particle density profile respects the symmetry contained in the external potential. Far away from any phase transition, the symmetry of the external field is expected to carry over to the density profile of the fluid. Phase transitions, however, can change the picture completely. One classic example of symmetry-breaking density profiles is the fluid freezing transition [1]. In the absence of any external potential, the density profile of the stable crystal consists of sharp peaks and is thus violating the full continuous translational symmetry of the (vanishing) field.

While the freezing transition is connected with a broken *continuous* symmetry the present paper is concerned with the possibility of breaking a *discrete* symmetry near the liquid-gas transition. Our model is motivated by the following considerations: One of the simplest external potential, $V_{ext}(z)$, z being a linear spatial coordinate, is that of an ''inverted sombrero,'' well known from quantum-field theory [2]

$$V_{ext}(z) = \Phi_0[(z/\lambda)^4 - (z/\lambda)^2], \qquad (1)$$

where Φ_0 sets an energy and λ a length scale. This double-well potential possesses the discrete inflection, or left-right symmetry

$$V_{ext}(-z) = V_{ext}(z). \qquad (2)$$

If one considers a classical fluid in this external potential far away from the freezing transition, it is strongly expected that the corresponding equilibrium-density profile reflects the symmetry of the external field. For instance, an ideal gas in an external potential exhibits a density profile

$$\rho(z) = \frac{1}{\Lambda^3} \exp\{[\mu - V_{ext}(z)]/k_B T\}, \qquad (3)$$

$k_B T$ denoting the thermal energy, Λ the thermal de Broglie wavelength, and μ the chemical potential. The density profile is thus always respecting the symmetry of the external potential. However, near a liquid-to-vapor transition, it is, at least in principle, conceivable that the system is in three different states: (1) liquidlike in the two wells, (2) vaporlike in the two wells, and (3) liquidlike in one and vaporlike in the other well. The last configuration is, of course, twofold degenerate and corresponds indeed to a density profile with broken discrete symmetry.

In order to reduce the complexity of the problem it is reasonable to introduce a simpler model by considering only two discrete values of the z coordinate. We discuss a double-slit model of two parallel plane layers of a two-dimensional liquid exhibiting a liquid-gas phase transition in the two-dimensional (2D) bulk. This system can be thought of as the limit of a double-well potential with infinitely deep minima. The two layers are coupled by an interlayer potential. One very familiar example is the two-dimensional Lennard-Jones liquid that exhibits a liquid-gas transition in the 2D bulk case [3,4] at a (temperature dependent) chemical potential μ_c. The possibility of discrete symmetry breaking near the liquid-gas transition is analyzed using density-functional theory and computer simulation. Within both approaches we establish the following results.

(i) If the net interaction V_0 between the two layers is attractive, $V_0 < 0$, then there is no symmetry breaking.

(ii) If the interaction V_0 is repulsive, both layers are in the vapourlike phase (i.e., no symmetry breaking) if the chemical potential μ is smaller than μ_c.

(iii) Symmetry breaking exists if the interlayer interaction is repulsive *and* the chemical potential is larger than that of coexistence, i.e., for $V_0 > 0$ and $\mu > \mu_c$.

Hence, symmetry breaking does occur. An experimental verification of this prediction is still ahead. Suitable samples are mesoscopic dispersions confined between parallel glass

---

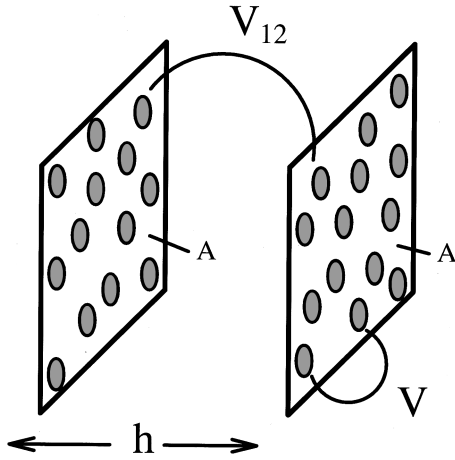*Also at Institut für Festkörperforschung, Forschungszentrum Jülich, D-52425 Jülich, Germany.

FIG. 1. Schematic view of the setup. Two two-dimensional slits with area A and distance h and corresponding in-plane potential $V(r)$ and interlayer interaction V_{12}.
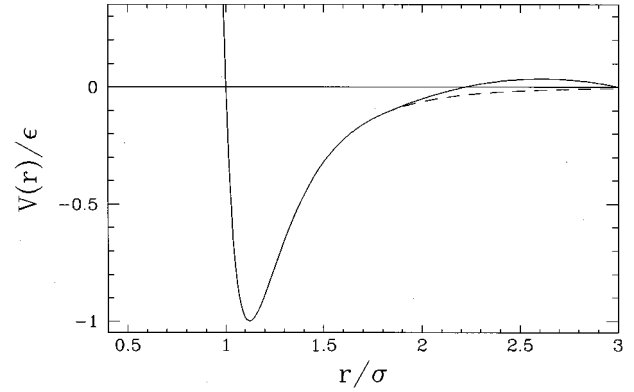

FIG. 2. Reduced interparticle potential $V(r)/\epsilon$ vs reduced distance r/σ: Lennard-Jones potential of model I (broken line) and Lennard-Jones potential with a parabolic well from model III (solid line). For $r<1.8\sigma$, the potentials are identical.

plates with added salt and added polymer [5]. In this system one can tailor the interparticle interaction by varying the salt concentration, the concentration of added polymer, and the quality of the solvent. Since our model is quite general one can expect that symmetry breaking does also occur in real samples.

Our work is organized as follows: In Sec. II we define the model. Then we turn to density-functional theory in Sec. III and to computer simulation of the density-functional input in Sec. IV. Results from density-functional theory are presented in Sec. V and results from computer simulation are discussed in Sec. VI. A discussion of a possible experimental verification of symmetry-breaking density profiles is finally done in Sec. VII.

II. THE MODEL

As already mentioned in the Introduction, we consider a double-slit system of two interacting parallel plane layers each of which contains a two-dimensional liquid. The separation of the layers is h and the layer area is A; the system is at a fixed finite temperature T and a given chemical potential μ. The setup is schematically shown in Fig. 1. The coordinates of the left plane are labeled by the index 1 and that of the right plane by index 2. Consequently the mean number density of particles in the left slit is $\rho_1=N_1/A$ while it is $\rho_2=N_2/A$ in the right one. The possible positions of the particles are $\vec{r}_1^{(i)}=(x_1^{(i)},y_1^{(i)},-h/2)$, $i=1,\ldots,N_1$ in the left and $\vec{r}_2^{(j)}=(x_2^{(j)},y_2^{(j)},h/2)$, $j=1,\ldots,N_2$ in the right slit.

In each layer, the particles interact via a 2D-pairwise potential $V(r)$, r denoting the 2D-interparticle distance. The interslit coupling is described by a radial symmetric pair potential $V_{12}(r)$, r denoting the distance between a particle from slit 1 to another particle from slit 2. Although we have studied cases where $V(r)\equiv V_{12}(r)$, we assume, in general, different $V(r)$'s and $V_{12}(r)$'s resulting in a set of three different models I, II, and III.

In our first model (model I) we take a truncated two-dimensional Lennard-Jones potential

$$V_{LJ}(r)=\begin{cases} 4\epsilon[(\sigma/r)^{12}-(\sigma/r)^6] & \text{for } r\leq r_c \\ 0 & \text{for } r>r_c \end{cases} \quad (4)$$

for *both* potentials $V(r)$ and $V_{12}(r)$. Here, ϵ sets an energy and σ a length scale and $r_c\equiv3\sigma$ is the cutoff distance. This potential is depicted in Fig. 2. It is a well-known two-dimensional model potential that was also studied for quite different topics as local liquid structure [6,7], freezing [8–11], and shear-induced aggregation [4].

A second model (model II) is defined by adopting the Lennard-Jones expression (4) for $V(r)$ and assuming a Yukawa form for $V_{12}(r)$:

$$V_{12}(r)=\begin{cases} \epsilon\dfrac{\sigma}{r}\exp(-\kappa r/\sigma) & \text{for } r\leq r_c \\ 0 & \text{for } r>r_c. \end{cases} \quad (5)$$

Here the dimensionless parameter $\kappa\equiv1$ determines the range of the interlayer coupling.

Finally in a third model (model III), we take $V_{12}(r)\equiv V(r)$ with

$$V(r)=\begin{cases} 4\epsilon[(\sigma/r)^{12}-(\sigma/r)^6] & \text{for } \leq1.8\sigma \\ \epsilon[-0.2275(r/\sigma)^2+1.1880(r/\sigma)-1.5154] \\ \qquad\qquad\qquad\qquad \text{for } 1.8\sigma<r\leq3\sigma \\ 0 & \text{for } r>3\sigma. \end{cases} \quad (6)$$

This potential, which is also shown in Fig. 2, is a Lennard-Jones potential with a repulsive parabolic well constructed in such a way that the potential and its first derivative are continuous at $r=1.8\sigma$.

Henceforth, we fix the temperature to be $T=0.45\epsilon/k_B$. For a truncated two-dimensional Lennard-Jones system (4), the triple temperature T_t is about $T_t=0.415\epsilon/k_B$ and the critical temperature T_c is about $T_c=0.533\epsilon/k_B$ [3]. These parameters are expected not to change drastically if a small repulsive well is added as in (6). Consequently, the chosen temperature guarantees that the system exhibits a first-order liquid-gas transition well separated from the critical point such that density fluctuations are rather small.
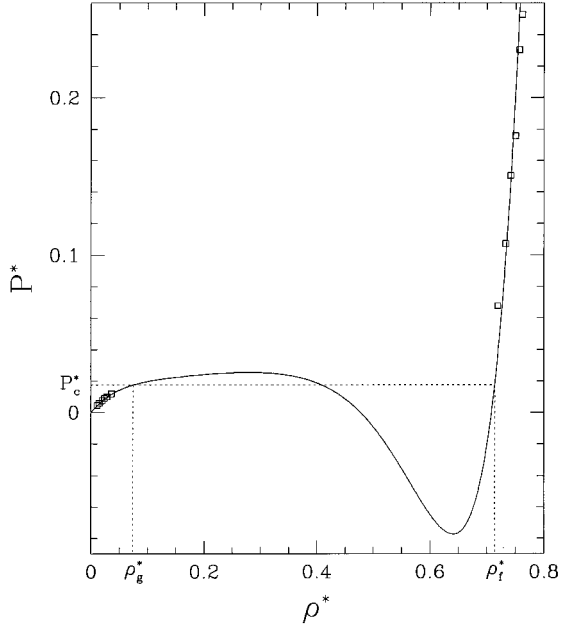
FIG. 3. Reduced pressure $P^* = P\sigma^2/\epsilon$ vs reduced density $\rho^* = \rho\sigma^2$ for a small system containing $N = 36$ particles. The solid line is an eighth-order polynomial fit to the simulation data. The van der Waals loop can clearly be seen and the coexisting pressure P_c^* and the coexisting densities ρ_g^* and ρ_f^* are indicated by the dotted lines. The open squares are data obtained from a grand canonical ensemble showing consistency with that from the canonical ensemble.

III. DENSITY-FUNCTIONAL THEORY

A. Theoretical framework

If we assume a homogeneous one-particle density distribution in both slits, we can write down a simple expression for the total Helmholtz free energy of the double-slit system by using density-functional theory [1]. The total free energy F is then a function of ρ_1 and ρ_2 and can be written as follows:

$$F(\rho_1,\rho_2) = F(\rho_1) + F(\rho_2) + F_{12}(\rho_1,\rho_2), \qquad (7)$$

where $F(\rho)$ is the free energy for a single slit and $F_{12}(\rho_1,\rho_2)$ describes the interaction between the slits. The quantity $F(\rho)$ can be readily obtained by computer simulation or liquid-state theory of a homogeneous two-dimensional bulk liquid. In fact we shall determine $F(\rho)$ by computer simulation in Sec. IV. The crucial part of the theory is the interaction term $F_{12}(\rho_1,\rho_2)$. We perform a mean-field theory [12,1] approximating

$$F_{12}(\rho_1,\rho_2) \approx \langle U_{12}\rangle = \rho_1\rho_2 \int_A d^2 r_1 \int_A d^2 r_2 g_{12}$$
$$\times (|\vec{r}_1 - \vec{r}_2|) V_{12}(|\vec{r}_1 - \vec{r}_2|). \qquad (8)$$

Here, U_{12} is the interlayer potential energy, $\langle\cdots\rangle$ denotes a canonical average and the interlayer pair correlation function $g_{12}(r)$ is defined via

$$g_{12}(r) = \frac{1}{\rho_1\rho_2} \left\langle \sum_{i=1}^{N_1} \sum_{j=1}^{N_2} \delta(x - x_1^{(i)}) \right.$$
$$\left. \times \delta(y - y_1^{(i)}) \delta(x_2^{(j)}) \delta(y_2^{(j)}) \right\rangle \qquad (9)$$

with $r = \sqrt{x^2 + y^2}$. Consequently we get within this mean-field approximation

$$F_{12}(\rho_1,\rho_2) = \rho_1\rho_2 A V_0, \qquad (10)$$

where the important constant V_0 embodies the globally averaged interlayer interaction

$$V_0 = 2\pi \int_h^{r_c} dr\, r g_{12}(r) V_{12}(r). \qquad (11)$$

It has to be noted that it is the single parameter V_0 that describes the slit-slit interaction in our theory.

Defining the free energy per particle $f(\rho) = F(\rho)/N$ and the grand canonical free energy per area $\omega(\rho) = \Omega(\rho)/A$ for the single-slit system, we can write down the following expression for the total grand canonical free-energy density $\omega(\rho_1,\rho_2) = \Omega(\rho_1,\rho_2)/A$:

$$\omega(\rho_1,\rho_2) = \omega(\rho_1) + \omega(\rho_2) + \rho_1\rho_2 V_0 = \rho_1 f(\rho_1) + \rho_2 f(\rho_2)$$
$$- \mu(\rho_1 + \rho_2) + \rho_1\rho_2 V_0. \qquad (12)$$

The actual values of the slit densities are now determined by *minimizing* $\omega(\rho_1,\rho_2)$ with respect to ρ_1 and ρ_2 at fixed T, A, and μ. Since $f(\rho)$ is a highly nonlinear function, in general the minimization has to be performed numerically. This will be done further in Sec. V.

B. Conditions for symmetry breaking

Before we proceed further let us do a preliminary analytical estimation. First we treat the case that the 2D bulk gas phase is stable which means $\mu < \mu_c$, μ_c denoting the chemical potential at liquid-gas coexistence. If ρ_1 is a density close to the bulk gas value and ρ_{12} another one close to a liquid value with

$$\rho_1 < \rho_2 \qquad (13)$$

we have $\omega(\rho_1) < \omega(\rho_2)$. Assume that a symmetry-breaking configuration with two different densities ρ_1 and ρ_2 is stable. Then it has lowest grandcanical free energy implying

$$\omega(\rho_1) + \omega(\rho_2) + \rho_1\rho_2 V_0 < 2\omega(\rho_1) + \rho_1^2 V_0 \qquad (14)$$

and

$$\omega(\rho_1) + \omega(\rho_2) + \rho_1\rho_2 V_0 < 2\omega(\rho_2) + \rho_2^2 V_0. \qquad (15)$$

Then we show that there is a contradiction. Indeed with $\Delta\omega \equiv \omega(\rho_2) - \omega(\rho_1) > 0$ we get from Eqs. (14) and (15)

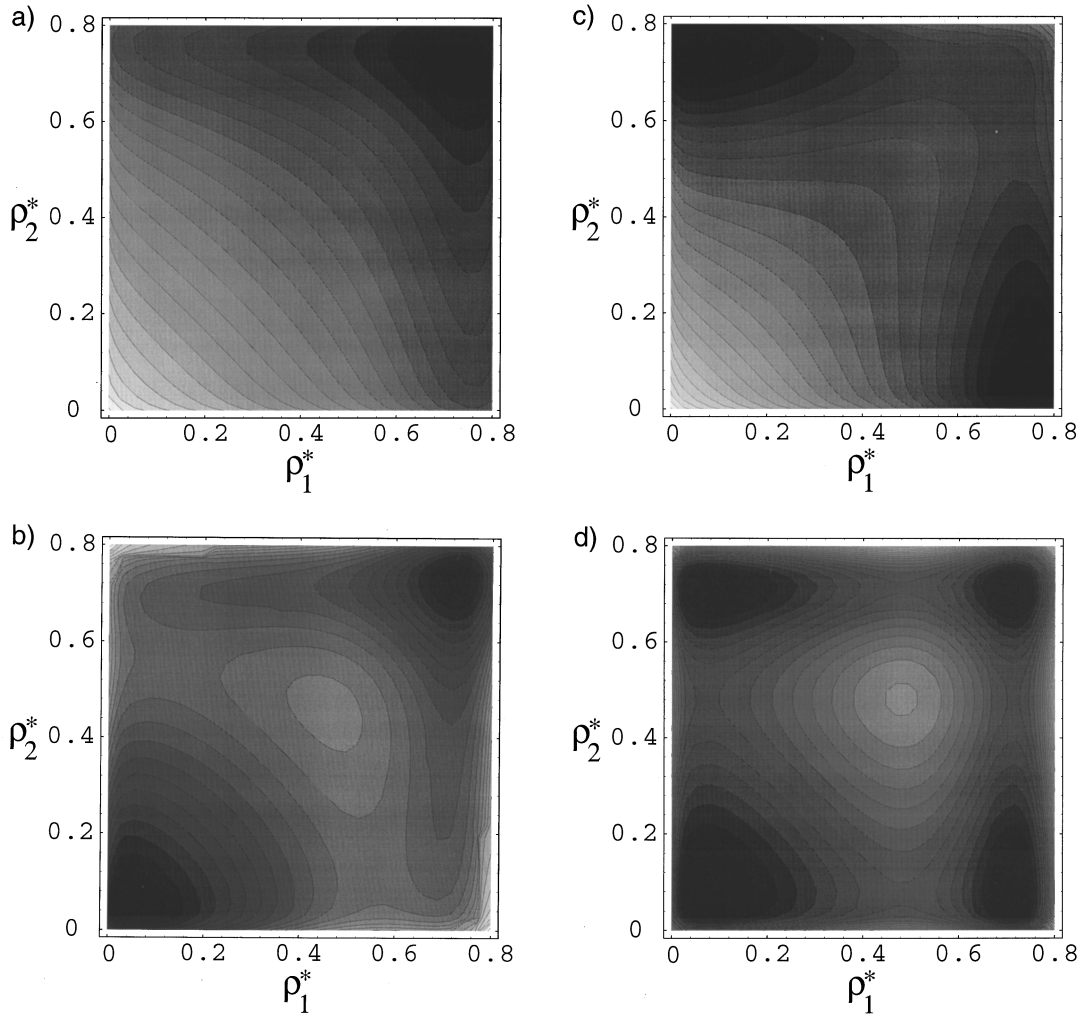$$-\frac{\rho_1}{\rho_2} < \frac{V_0\rho_1(\rho_2 - \rho_1)}{\Delta\omega} < -1, \qquad (16)$$

FIG. 4. Equipotential lines for the grand canonical free energy $\omega(\rho_1,\rho_2)$ in the space spanned by the reduced densities $\rho_1^* = \rho_1\sigma^2$ and $\rho_2^* = \rho_2\sigma^2$ for models I and II. A darker region corresponds to a lower free energy. (a) Liquid-liquid situation, $V_0 = 0.25\epsilon$, $\Delta\mu = 0.4\epsilon$. (b) Gas-gas situation, $V_0 = -0.25\epsilon$, $\Delta\mu = -0.1\epsilon$. (c) Situation with broken symmetry, $V_0 = 0.7\epsilon$, $\Delta\mu = 0.4\epsilon$. (d) Coexistence situation, $V_0 = 0$, $\Delta\mu = 0$.

which necessarily implies $\rho_1 > \rho_2$ in contradiction to our assumption (13). This consideration proves that there is no symmetry breaking within our theory for $\mu < \mu_c$.

Next, in the case $\mu > \mu_c$ where the liquid is stable a similar consideration with $\Delta\omega < 0$ yields

$$-\frac{\rho_1}{\rho_2} > \frac{V_0\rho_1(\rho_2 - \rho_1)}{\Delta\omega} > -1. \qquad (17)$$

Hence, once ρ_1, ρ_2, and $\Delta\omega$ are given, there is a certain range of positive values for V_0 where these conditions are satisfied while they can never be satisfied for negative V_0.

To summarize: Symmetry-breaking density profiles can only occur for $\mu > \mu_c$ and for repulsive interlayer couplings $V_0 > 0$. This establishes the first important result of our paper. The only approximations are the mean-field approach (8) which ignores entropy contributions to the free energy stemming from a fluctuating liquid-gas interface inside the layers and the assumption that there is no freezing transition. Indeed the symmetry-breaking region in μV_0 space can be preempted by a further phase transition (e.g., freezing) which

is not incorporated into our model. We shall check the validity of these two assumptions later on by computer simulation. In fact, while the mean-field theory always seems to be justified, it is possible that an underlying freezing transition spoils the relative simplicity of our theory.

IV. COMPUTER SIMULATION FOR THE DENSITY-FUNCTIONAL INPUT

The main requisite for our theory is a knowledge of the function $f(\rho)$ depending on the interparticle forces (4) and (6). This is achieved using Monte Carlo (MC) simulation of *one* slit in the canonical *NAT* ensemble. We use a square with periodic boundary conditions containing a small number of $N = 36$ particles. At least 6×10^5 MC steps per particle were done to perform statistical averages. Using the virial expression in two dimensions [13], the pressure P was obtained for varying particle number densities ρ. Looking for a van der Waals loop in $P(\rho)$, the gas-liquid phase transition was located by performing a Maxwell construction. Finally
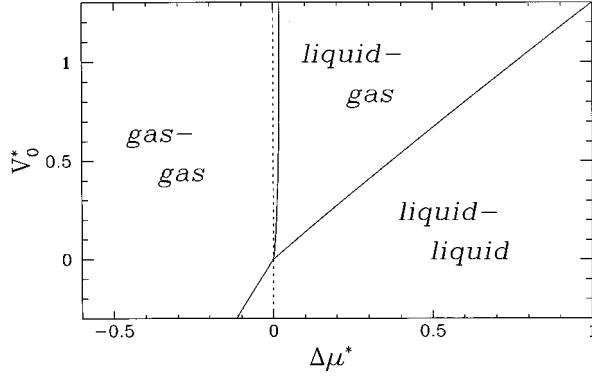
FIG. 5. Phase diagram in the plane of reduced chemical potential difference $\Delta\mu^* = (\mu - \mu_c)/\epsilon$ and reduced interlayer coupling $V_0^* = V_0/\epsilon$ for models I and II. The solid lines are the phase boundaries as obtained from density-functional theory. The vertical dotted line corresponds to $\Delta\mu = 0$.

the free-energy density $f(\rho)$ was obtained by integrating $P(\rho)$ along an isotherm as

$$f(\rho) = \int_{\rho_0}^{\rho} d\rho' \, \frac{P(\rho')}{\rho'^2} + f(\rho_0). \qquad (18)$$

Here the constant f_0 was determined by matching the result to the well-known dilute ideal-gas limit

$$f(\rho) = k_B T[\ln(\Lambda^3 \rho) - 1] \qquad (19)$$

as $\rho \to 0$, Λ denoting the de Broglie thermal wavelength. The reason to take a relatively small system ($N = 36$) was to avoid internal liquid-gas phase boundaries in the system that reduces the magnitude of the van der Waals loop. Since we shall use $f(\rho)$ as a density-functional input where such fluctuations are ignored, one has to enforce this by simulating a small system size. In fact, simulations with a higher number of particles ($N = 256$) shows that the loop magnitude is reduced although the values of the coexisting densities and pressures did not change. In order to check consistency of our simulations, we have also used the grand canonical μAT ensemble where the chemical potential μ is prescribed using the method of Mezei [14] with a neighbor-list method [15]. Indeed, we found consistency with the simulations in the canonical ensemble. For more details, we refer to [16].

Explicit results for the truncated Lennard-Jones potential (4) relevant for models I and II are shown in Fig. 3. Note that the pressures occurring during the van der Waals loop can be negative although the physical coexisting pressures have to be positive. Also it is demonstrated that the data obtained from the grand canonical ensemble (open squares) coincide with that from the canonical ensemble showing consistency of our simulations in different ensembles. The coexisting pressure is $P_c = 0.017\epsilon/\sigma^2$ while the coexisting gas and liquid densities turn out to be $\rho_g = 0.074/\sigma^2$ and $\rho_f = 0.71/\sigma^2$. Furthermore, the chemical potential at coexistence,

$$\mu_c = f(\rho_g) + \rho_g \, \frac{df(\rho_g)}{d\rho} \equiv f(\rho_f) + \rho_f \, \frac{df(\rho_f)}{d\rho}, \qquad (20)$$
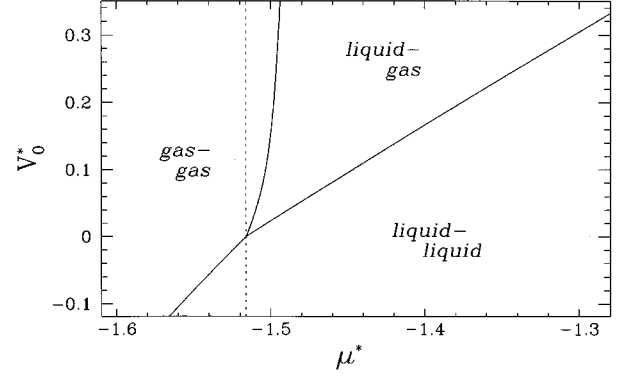

FIG. 6. Same as Fig. 5 but now for model III.

is -1.715ϵ provided the de Broglie thermal wavelength Λ is set to σ. For the slightly changed potential (6) in model III, we obtain $P_c = 0.029\epsilon/\sigma^2$, $\rho_g = 0.182/\sigma^2$, $\rho_f = 0.683/\sigma^2$, and $\mu_c = -1.516\epsilon$ again with $\Lambda \equiv \sigma$.

V. RESULTS FROM DENSITY-FUNCTIONAL THEORY

Once we have determined the Helmholtz free energy per particle $f(\rho)$ in the homogeneous bulk phases, we can evaluate explicitly our density-functional theory from Sec. III. Plotting the key quantity $\omega(\rho_1, \rho_2)$ which has to be minimized with respect to ρ_1 and ρ_2, we get qualitatively different situations for different values of μ and V_0. For models I and II we have shown four cases in Figs. 4(a)–4(d) in the ρ_1-ρ_2 plane. The darker the region the smaller is the value of $\omega(\rho_1, \rho_2)$. In Figs. 4(a) and 4(b), the minimum occurs on the diagonal meaning that it occurs for $\rho_1 \equiv \rho_2$, i.e., there is no symmetry breaking. In fact, in Fig. 4(a) ($V_0 = 0.25\epsilon$, $\Delta\mu = 0.4\epsilon$) the minimum corresponds to a liquid-liquid situation in the two slits with a density that is close to the coexisting liquid density. This shows that the necessary conditions for symmetry breaking $V_0 > 0$ and $\Delta\mu > 0$ as obtained from Sec. III B are indeed not sufficient. On the other hand, in Fig. 4(b) ($V_0 = -0.25\epsilon$, $\Delta\mu = -0.1\epsilon$) there is a gas-gas situation as expected from our considerations in Sec. II B. In Fig. 4(c) we have shown a situation with $V_0 = 0.7\epsilon$ and $\Delta\mu = 0.4\epsilon$, again fulfilling the necessary conditions for symmetry breaking from Sec. III B. Here we really see that the minimum is off-diagonal, which implies a symmetry-broken density. Finally, in Fig. 4(d), the situation of coexistence is shown ($V_0 \equiv 0$, $\Delta\mu = 0$) where the two symmetric situations coexist with the symmetry-broken situation.

The whole phase diagram is shown in Fig. 5 for more models I and II and in Fig. 6 for model III showing the stability of the three situations, gas-gas, liquid-liquid, and gas-liquid versus $\Delta\mu$ and V_0. As predicted from our estimation in Sec. III B the symmetry-broken situation occurs only for $V_0 > 0$ and $\Delta\mu > 0$. Furthermore, the topology of the phase diagrams of the I and II models and of the III model are quite similar.

We finally remark that it is *a priori* unclear whether the full V_0 scale is realized in a concrete model. As is clear from the definition (11), this depends on the explicit form of the interlayer potential $V_{12}(r)$ as well as on the pair correlation function $g_{12}(r)$. Since a calculation of $g_{12}(r)$ requires a detailed liquid-state analysis for the coupled two-slit model, we

TABLE I. Parameters and results for three different runs (a), (b), and (c) for model I. Given are the system size $A^* = A/\sigma^2$, the reduced chemical potential $\mu^* = \mu/\epsilon$, the reduced plate distance $h^* = h/\sigma$, the reduced interlayer coupling $V_0^* = V_0/\epsilon$ obtained from Eqs. (11) and (21), as well as the reduced densities in the two slits as obtained from simulation (MC) and density-functional theory (DFT).

Run	A^*	μ^*	h^*	V_0^*	ρ_1^* (MC)	ρ_2^* (MC)	ρ_1^* (DFT)	ρ_2^* (DFT)
(a)	3600	-2.1	1.811	-0.5	0.0113	0.0113	0.0144	0.0144
(b)	576	-1.32	1.811	-0.5	0.816	0.807	0.790	0.790
(c)	576	-1.32	0.848	1.0	0.831	0.830	0.0149	0.7624

henceforth approximate further by assuming

$$g_{12}(r) \approx \Theta(r-h), \qquad (21)$$

$\Theta(x)$ denoting the unit step function. Then V_0 is directly given as the lateral integral of the interaction $V_{12}(r)$.

VI. RESULTS FROM COMPUTER SIMULATION OF THE MODEL

We have done Monte Carlo simulations for the full coupled two-slit model in the grand canonical ensemble using the cavity-biased method of Mezei [14,16]. The system was a square with periodic boundary conditions with an area ranging between $81\sigma^2$ and $3600\sigma^2$. The length of a simulation run after equilibration was typically 4×10^6 Monte Carlo steps per particle. The three different models were subsequently studied.

A. Results for model I

Three different runs (a), (b), and (c) were performed, the parameters of which are summarized in Table I. The corresponding value of V_0 was calculated using the approximation (21) and is also included in Table I. The theory predicts a symmetric profile for runs (a) and (b) and a broken symmetry for run (c). In fact, the resulting slit densities are in good agreement with the simulation data in the symmetric case but fail completely for run (c), see Table I.

In order to explore the microscopic reason for this discrepancy we have first checked the assumption (21). The simulated interlayer pair correlation functions $g_{12}(r)$ are shown in Fig. 7. While the approximation $g_{12}(r) \approx 1$ turns out to be valid in the symmetric case, there are strong correlations for run (c) proving that the approximation (21) breaks down. In fact, if one recalculates V_0 based upon Eq. (11) with the simulated $g_{12}(r)$ one gets $V_0 = -0.581\epsilon$ for run (a) and $V_0 = -0.504\epsilon$ for run (b) which are close to -0.5ϵ as predicted by the approximation (21). For run (c), however, one gets $V_0 = -4.52\epsilon$ instead of the old value $V_0 = \epsilon$, i.e., even the sign changes. Now if one recalculates the slit densities with this new value of V_0 one gets a symmetric situation with $\rho_1 = \rho_2 = 0.890\sigma^2$, which is still not in agreement with the simulation. The microscopic reason for that becomes clear if one plots a typical particle configuration of the MC simulation, see Fig. 8. One sees a clear ordering into two intersecting triangular lattices in the two slits. Two neighboring particles from different slits are basically located in the Lennard-Jones minimum of $V_{12}(r)$ that is also reflected by the high peak in $g_{12}(r)$. This finally results in freezing. Since the freezing transition is not incorporated into our simple

density-functional approach, the theory fails in predicting the correct slit densities.

To summarize: There is no symmetry breaking in model I since it was preempted by the freezing transition. As long as one is in a symmetric situation, liquid-liquid or gas-gas, the slit densities are in quantitative agreement with the theory.

B. Results for model II

In model II, the interlayer interaction (5) is purely repulsive. Hence it is expected that a freezing transition due to particle aggregation in the minima of $V_{12}(r)$ is suppressed. Indeed, our theoretical analysis was completely confirmed by computer simulation.

In order to check the theoretical predictions, we performed a set of MC simulations in the $\Delta\mu V_0$ plane. We remark that the simulations were done for different h; V_0 was then determined by adopting Eqs. (21) and (11). A system size of $A = 576\sigma^2$ was used. We started with three different initial configurations corresponding to liquid-liquid, gas-gas, and liquid-gas situations in order to check consistency of the final result and to see effects of hysteresis directly. The results are summarized in Fig. 9. An open square in Fig. 9 means that the system relaxes to the same situation irrespective of the initial configuration. This gives strong support that equilibrium was reached within the duration of the simulation. In fact, if the final situation was unique, it did agree with the theoretical prediction [again with V_0 obtained from Eq. (21)]. A cross in Fig. 9 means that the system exhibited hysteresis effects during the simulation. This can be interpreted as bars of the statistical error in the location of
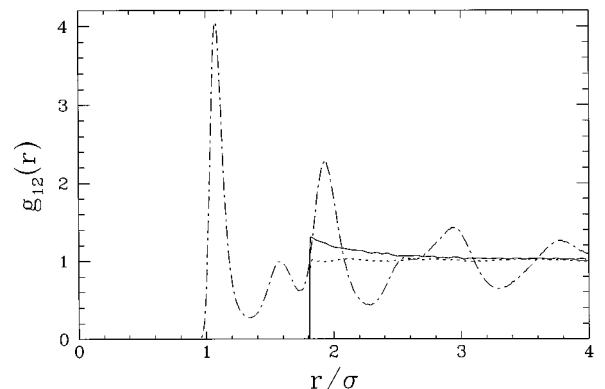

FIG. 7. Interlayer pair correlation function $g_{12}(r)$ vs reduced distance r/σ for model I: run (a) (solid line), run (b) (dotted line), and run (c) (dot-dashed line).
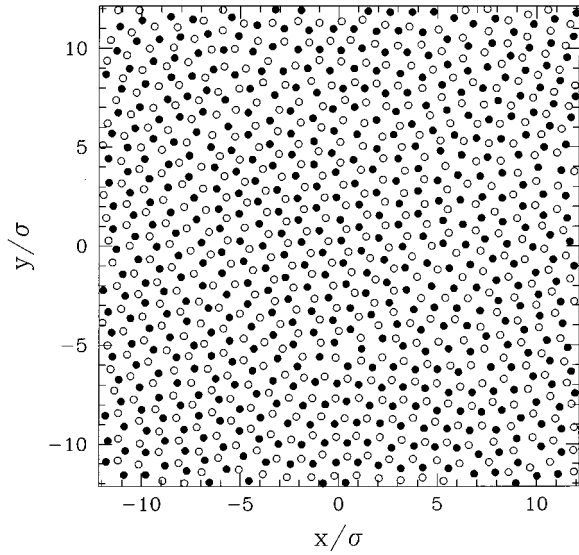
FIG. 8. Particle positions projected onto the xy-slit plane for model I [run (c)]. The particles of slit 1 are black while that of slit 2 are represented by open circles. In this snapshot, $N_1=486$ and $N_2=487$.

the phase boundary. At least for the series of runs presented, the phase boundaries of the theory were excellently reproduced by the simulation. In particular, symmetry-breaking density profiles do occur as predicted by theory. In Fig. 10 a typical snapshot of particle positions is shown, clearly exhibiting a gas-liquid situation. Moreover, we have compared the slit densities with the theoretical values in Figs. 11 and 12. Again, the agreement was quantitatively correct.

Finally we have investigated the stability of a coexisting situation in one slit for the liquid-gas situation. As an initial configuration, we have chosen a liquid drop surrounded by its gas in one slit and the complementary setup (gas bubble surrounded by a liquid) in the other slit. Of course creating an interface in a slit costs a line tension but it is *a priori* not clear whether the higher entropy of fluctuating islands can result in a symmetric situation. In other terms, such an effect would imply that our mean-field approximation (8) has broken down. We have taken a very large sample with an area

FIG. 10. Snapshot of a configuration, the symmetry-breaking regime. Particle position in the xy plane for (a) the left slit and (b) the right slit. The parameters are $\mu=-1.32\epsilon$ and $V_0=1.0\epsilon$ (model II).

of $A=1764\sigma^2$ and monitored snapshots during the simulation in Fig. 13. We observed that the drop was not stable but disappeared. This demonstrates that interface fluctuations, at least on the length scale prescribed by the system size, do not change symmetry-breaking density profiles. This is, in fact, expected since the underlying liquid-gas transition is strongly first order and fluctuations are expected not to play any role. The situation, of course, may drastically change for temperatures close to the critical point.

C. Results for model III

Once we have established symmetry breaking in model II, one may ask whether it also occurs in a more realistic model where $V(r)\equiv V_{12}(r)$. In fact, adopting model III, we found, again, that symmetry breaking occurred. The results of computer simulations again coincided with that gained from
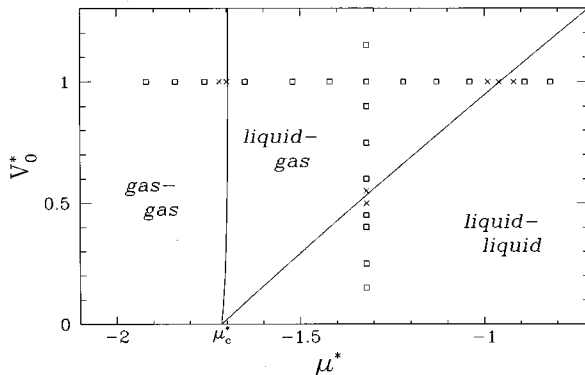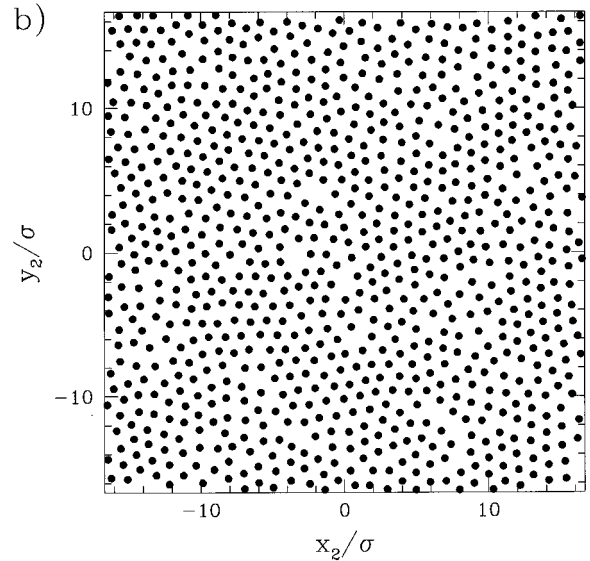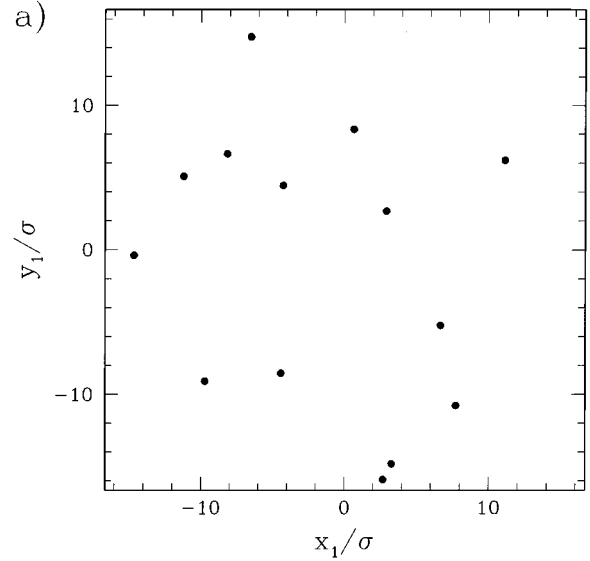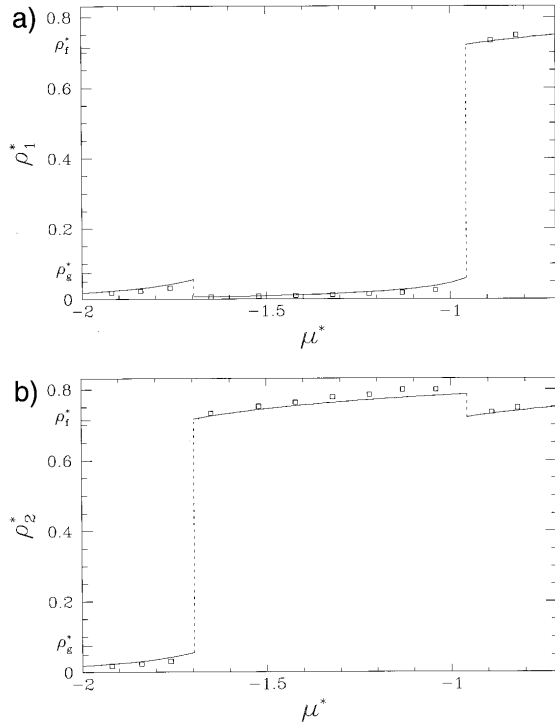

FIG. 9. Same as Fig. 5 but now with the results of computer simulation. The open square means a unique final configuration that coincides with that predicted by density-functional theory. A cross means that the final configuration depends on the initial guess.

FIG. 11. Reduced densities (a) in the first slit ρ_1^*, (b) in the second slit ρ_2^*, vs reduced chemical potential μ^* for constant value of $V_0 = \epsilon$. The open squares are the results of the MC simulation while the solid lines are that obtained from density-functional theory.

FIG. 12. Same as Fig. 11 but now for fixed chemical potential $\mu = -1.32\epsilon$ and varying V_0.

density-functional theory. The only difference was that fluctuations were a bit more pronounced since the temperature was a bit closer to the critical one. For the explicit results and for more details, we refer to [16].

VII. DISCUSSION AND OUTLOOK

In order to verify the predicted symmetry-breaking density profiles in real samples, we suggest observations on mesoscopic colloidal particles suspended in a solvent and confined between two parallel plates. The external potential $V_{ext}(z)$, z being the coordinate perpendicular to the walls, is governed by the wall-particle interaction. In fact, the van der Waals attraction [17,5,18] between the walls and the particles leads to two deep symmetric minima near wall contact. The strength of this interaction can be tuned by varying the nature of the solvent. Assuming that the particles are mainly captured in these two minima, we can justify the applicability of our simple-slit model. Next, the interparticle forces need to have an attraction between particles from the same slit (in order to exhibit a liquid-gas transition) and a repulsion between particles from different slits (in order to avoid freezing). Possible realizations are sterically stabilized suspensions that are additionally low charged with added polymer in the solution. The steric stabilization induces a strong short-ranged repulsion; the added polymer leads to an effective attraction on a slightly longer-ranged length scale and the weakly screened charge finally results in long-ranged repulsion. Neglecting the particle-particle van der Waals attraction, the qualitative structure of the resulting $V(r)$ is very
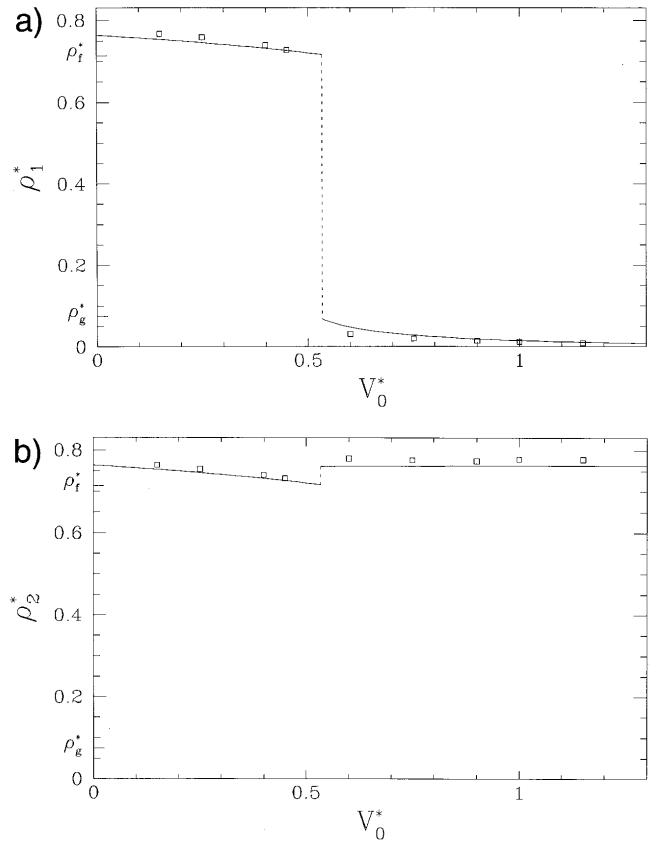
much similar to that assumed in our model III. An explicit difference between $V(r)$ and $V_{12}(r)$ can be obtained by applying an electric or magnetic field perpendicular to the plates that induces dipoles in the particles resulting into an anisotropic effective interaction which was assumed in model II. Hence, at least in principle, experimental realizations of our models are conceivable.

In conclusion, we have established, by computer simulation and density-functional theory, that a system confined in a symmetric external potential can exhibit density profiles that break the symmetry of the external potential. Explicit results were obtained, near the two-dimensional liquid-to-gas transition, in a simple two-slit model. We reemphasize that the discrete symmetry contained in the external potential $V_{ext}(z)$ can or cannot be broken depending delicately on the nature of the interparticle potential $V_{12}(r)$. Also, it seems indeed to be possible to verify the predicted discrete symmetry breaking experimentally. In an experiment on confined colloids one would notice symmetry-breaking density profiles by watching the particle configurations in real space using video microscopy (see, e.g., [19]) ending up with pictures that are identical to our snapshots gained from the computer simulation. Another possibility to extract the colloidal density profile is light scattering [20].

We finish with a couple of remarks: First, it would be interesting to explore the disappearance of symmetry-breaking density profiles and the associated scaling behavior if the temperature is enhanced towards the critical point.
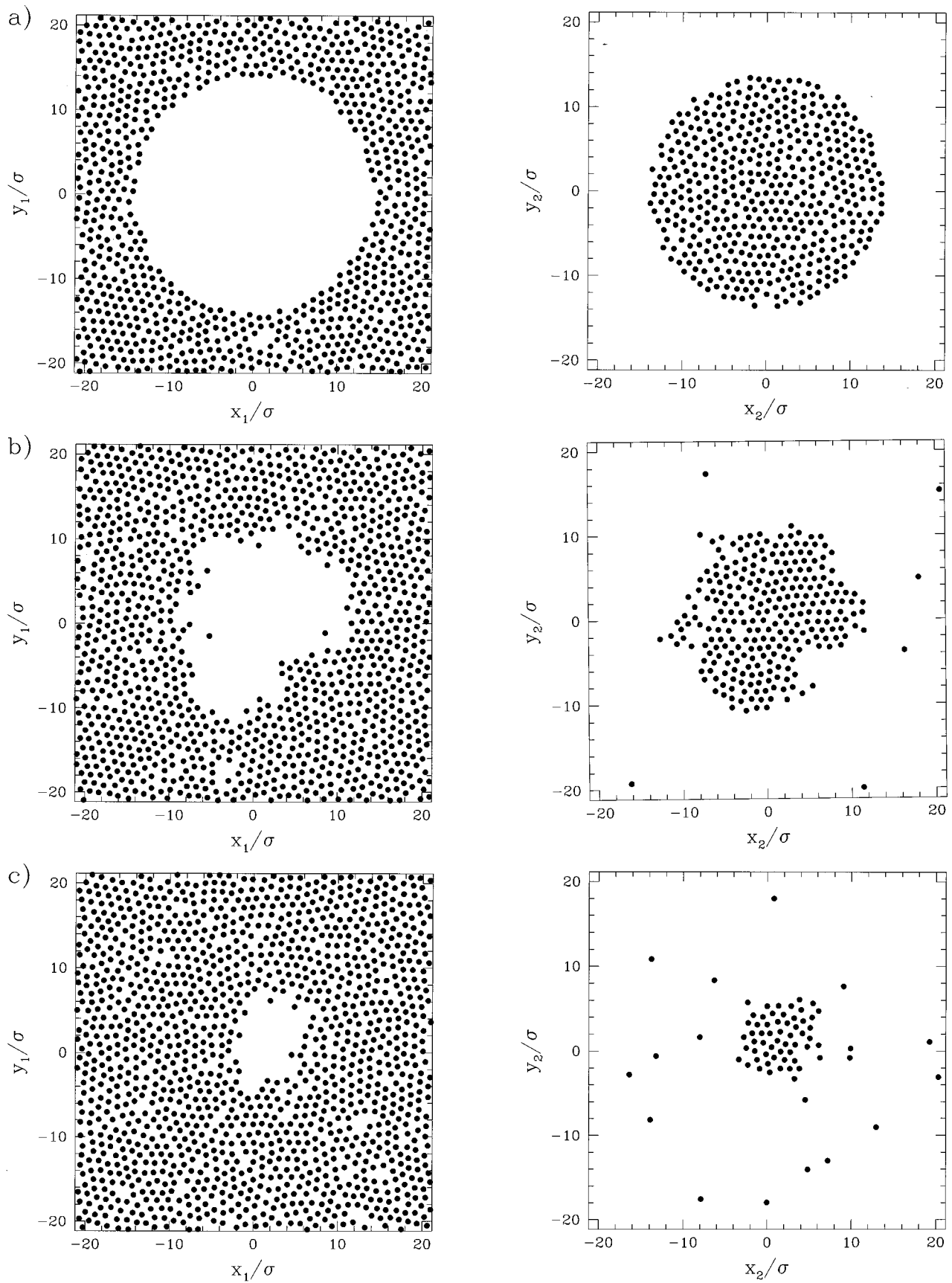
FIG. 13. Snapshot of typical particle configurations in the left and right slit during the MC simulations starting from a droplet configuration with interface (model II). The parameters are $\mu = -1.32\epsilon$ and $V_0 = \epsilon$. (a) Initial configuration, the droplet occupies 35% of the total area. (b) After 1.6×10^6 MC moves. (c) After 3.2×10^6 MC moves. Here the symmetry-breaking equilibrium was nearly reached.

Second, we would like to point out that the freezing transition in an external potential of parallel confining walls also breaks the discrete symmetry if the crystalline phase is buckled or unsymmetrically layered [21].

[1] H. Löwen, Phys. Rep. **237**, 249 (1994).

[2] C. Itzykson and J.-B. Zuber, *Quantum Field Theory* (McGraw-Hill, New York, 1985), p. 522.

[3] F. F. Abraham, Phys. Rep. **80**, 340 (1980).

[4] B. D. Butler, H. J. M. Hanley, D. Hansen, and D. J. Evans, Phys. Rev. B **53**, 2450 (1996).

[5] W. B. Russel, D. A. Saville, and W. R. Schowalter, *Colloidal Dispersions* (Cambridge University Press, Cambridge, 1989).

[6] A. C. Mitus, A. Z. Patashinskii, and S. Sokolowski, Physica A **174**, 244 (1991).

[7] R. Yamamoto and K. Nakanishi, Phys. Rev. B **51**, 2715 (1995).

[8] S. Toxvaerd, Phys. Rev. A **24**, 2735 (1981).

[9] J. Tobochnik and G. V. Chester, Phys. Rev. B **25**, 6778 (1982).

[10] A. F. Bakker, C. Bruin, and H. J. Hilhorst, Phys. Rev. Lett. **52**, 449 (1984).

[11] C. Udink and J. van der Elsken, Phys. Rev. B **35**, 279 (1987).

[12] S. Dietrich, in *Phase Transitions and Critical Phenomena*, edited by C. Domb and J. Lebowitz (Academic, London, 1988), Vol. 12, p. 1.

[13] H. Löwen, J. Phys. Condens. Matter **4**, 10 105 (1992).

[14] M. Mezei, Mol. Phys. **40**, 901 (1980).

[15] See, e.g., M. P. Allen and D. J. Tildesley, *Computer Simulation of Liquids* (Clarendon, Oxford, 1989).

[16] M. Merkel, Diploma thesis, University of Munich, Germany, 1996 (unpublished).

[17] E. J. W. Verwey and J. T. G. Overbeek, *Theory of the Stability of Lyophobic Colloids* (Elsevier, Amsterdam, 1948).

[18] P. N. Pusey, in *Liquids, Freezing and the Glass Transition*, edited by J. P. Hansen, D. Levesque, and J. Zinn-Justin (North-Holland, Amsterdam, 1991).

[19] C. A. Murray and D. H. van Winkle, Phys. Rev. Lett. **58**, 1200 (1987); C. A. Murray, W. O. Sprenger, and R. A. Wenk, Phys. Rev. B **42**, 688 (1990); A. H. Marcus, B. Lin, and S. A. Rice, Phys. Rev. E **53**, 1765 (1996).

[20] N. A. Clark, B. J. Ackerson, and A. J. Hurd, Phys. Rev. Lett. **50**, 1459 (1983).

[21] M. Schmidt and H. Löwen, Phys. Rev. Lett. **76**, 4552 (1996).